Conf-901073-12

Second Harmonic Generation and Sum Frequency Generation*

M. J. Pellin, B. M. Biwer, M.W. Schauer**, J. M. Frye***
and D. M. Gruen

Materials Science and Chemistry Divisions
Argonne National Laboratory
Argonne, Illinois 60439

CONF-901073--12

DE91 006654

Second harmonic generation and sum frequency generation are increasingly being used as *in situ* surface probes. These techniques are coherent and inherently surface sensitive by the nature of the mediums response to intense laser light. Here we will review these two techniques using aqueous corrosion as an example problem. Aqueous corrosion of technologically important materials such as Fe, Ni and Cr proceeds from a reduced metal surface with layer by layer growth of oxide films mitigated by compositional changes in the chemical makeup of the growing film. Passivation of the metal surface is achieved after growth of only a few tens of atomic layers of metal oxide. Surface Second Harmonic Generation and a related nonlinear laser technique, Sum Frequency Generation have demonstrated an ability to probe the surface composition of growing films even in the presence of aqueous solutions.

I. Introduction. Aqueous corrosion of technologically important materials such as Fe, Ni and Cr proceeds from a reduced metal surface with layer by layer growth of oxide films mitigated by compositional changes in the chemical makeup of the growing film. Passivation of the metal surface is achieved after growth of only a few tens of atomic layers of metal oxide. A microscopic understanding of the composition and structure of these growing films has been lacking due to the difficulties associated with sensitive, *in situ*, analysis at the water metal interface. Monolayer or near-monolayer sensitivity is required since electrochemically grown films are complicated inhomogeneous structures which are, in total, no more than 30 atomic layers thick. It is at the single monolayer level that compositional changes make themselves felt. Furthermore, it is at the monolayer level that the effects of trace water contaminants such as halogens, sulfates, and borates can be expected to exert their strongest influence on the corrosion process.

Recently, a new technique, surface second harmonic generation (SSHG) and its companion sum frequency generation (SFG), are being developed which can probe

---

* Work supported by the U.S. Department of Energy, BES-Materials Sciences, under Contract W-31-109-ENG-38.

** Present address: Department of Chemistry, University of North Carolina (Chapel Hill), Chapel Hill, NC 27599-3290

*** Present address: Department of Chemistry, Howard University, Washington, DC 20059

the growing metal oxide film *in situ*. The SSHG technique involves a second order nonlinear process in which two incident photons of frequency, ω_1, are converted to one photon of frequency, $2\omega_1$. A distinct advantage of the technique is that generation of signal photons (in the electric dipole approximation) is forbidden in media with inversion symmetry. In an electrochemical cell, this means that any signal detected must have arisen from the electrode surface. Recent studies have extended the use of SSHG to technologically important materials such as Fe and Ni which have intrinsically low SSHG signal generation coefficients by utilizing picosecond laser technology.[1-4,57] Picosecond laser pulses have the high *intensity* required for efficient SSHG generation while minimizing deleterious sample heating effects which result from light pulses with large *energies*.

The information derived from SSHG or SFG is similar to an absorption spectrum of a submonolayer film, but it is richer in two ways. First, both one- and two-photon resonances are detected. Recently, this property of SFG has been used with one tunable infrared photon and one visible photon, simultaneously allowing the measurement of the vibrational absorption spectrum of a Ni surface using high quantum efficiency visible photon detection.[5] Second, the absorption event is tensor in nature (i.e., depends on the polarization of both the two incoming photons and on the surface and bulk symmetry of the substrate), so structural information can be derived from polarization and angle of incidence studies. The symmetry of metal and semiconductor surfaces has been observed in ultrahigh vacuum (UHV) environments, with and without adsorbates using this technique.[3,5-10] Also, the symmetry of a silver electrode has been monitored *in situ* as electrochemical processes occur.[11,12]

SSHG is, therefore by its very nature, ideally suited as an *in situ* surface probe. The SSHG signal is free of bulk contributions in the dipole approximation . Moreover, the SSHG signal is carried on a coherent beam allowing measurements to be made in extremely harsh environments. Several extensive reviews have been published on the SSHG technique in recent years and may be refered to for additional detail.[49,50,63,64] This paper is intended to acquaint the reader with the SSHG technique and focus on its *in situ* aspects. As examples of the use of SSHG in the study of environmental/materials interactions let us examine two specific systems - the air oxidation of Fe [110] single crystal,[3] and Ni passivation in acid chloride solutions.[4]

II. Theory. The origins of SHG are found in the second order non-linear polarization of a material, $\vec{P}_{nl}^{(2)}$, when induced by an incoming electromagnetic plane wave with frequency ω. The form of $\vec{P}_{nl}^{(2)}$ in an isotropic medium is given in equation 1 where $\vec{E}(\omega)$ and $\vec{B}(\omega)$ are the electronic and magnetic fields of the incoming radiation.[13]

$$\vec{P}_{nl}^{(2)} = (2i\,\omega/c)\,\gamma\,[\vec{E}(\omega) \times \vec{B}(\omega)] + (\delta-\beta)\,[\vec{E}(\omega)\cdot\vec{\nabla}]\,\vec{E}(\omega)$$

$$+ \beta\ \vec{E}(\omega)\,[\vec{\nabla}\cdot\vec{E}(\omega)] + \chi^{(2)} : \vec{E}(\omega)\vec{E}(\omega) \qquad (1)$$

$\chi^{(2)}$ is the microscopic second order electric susceptibility and is a tensor of rank three. β, δ, and γ are frequency dependent parameters which are material dependent. The generated second harmonic fields are found by solving the wave equation using $\vec{P}_{nl}^{(2)}$, equation 2.[14,15]

$$\vec{\nabla} \times \vec{\nabla} \times \vec{E}_2 + \frac{\vec{\varepsilon}(2\omega)}{c}\,\frac{\partial^2 E_2}{\partial t^2} = -\frac{4\pi}{c^2}\,\frac{\partial^2 P_{nl}^{(2)}}{\partial t^2} \qquad (2)$$

The reflected SHG intensity is then calculated to be that shown in equation 3.[13,16]

$$I(2\omega) = \frac{3\,2\pi^3\,\omega^2\,\sec^2\theta_{2\omega}}{c^3\,\varepsilon_1(\omega)\,\varepsilon_1^{1/2}(2\omega)}\,|\vec{e}_{2\omega}\cdot\vec{\chi}_{eff}^{(2)}:\vec{e}_{\omega}\vec{e}_{\omega}|^2\,I^2(\omega) \qquad (3)$$

$\vec{\varepsilon}_1$ is the dielectric constant for the incident medium, $\vec{e}(\omega)$ and $\vec{e}(2\omega)$ are related to the polarization vectors for the light at the given frequency, and $\theta_{2\omega}$ is the angle between the SSHG signal in the reflected direction and the surface normal. Note that the second harmonic intensity is proportional to the square of the incident intensity.

$\chi^{(2)}_{eff}$ incorporates contributions from all four terms given in equation 1. The first three terms are important when dealing with electron free gas (e.g. metals due to the presence of delocalized electrons). The first term arises from the classical Lorentz force on conduction electrons and is the bulk magnetic dipole contribution to SHG. The second and third terms are electric quadruple contributions. However, the second term vanishes when excitation is due to a single plane wave. The third term, again a result of conduction electrons, vanishes in a homogeneous medium, but does exist across an interface between two dissimilar materials. Therefore, the third term gives a surface sensitive contribution to the SHG signal, and a bulk contribution when dealing with certain crystalline structures. The second order electric susceptibility, $\chi^{(2)}$, is the fourth term component shown in equation 1 for the $\vec{P}_{nl}^{(2)}$. $\chi^{(2)}$ vanishes in a medium with inversion symmetry and exists only at the interface between two homogeneous media in the electric dipole approximation. In the case of non-centrosymmetric media, $\chi^{(2)}$ will

also have a bulk contribution. The directional properties of $\chi^{(2)}$ make SHG an ideal surface/bulk structural probe for certain materials when in situ measurements are necessary. Using perturbation theory, $\chi^{(2)}$ can be shown to be of the form shown in equation 4.

$$\chi^{2} \propto \frac{\Sigma \mu_{gi} \mu_{ij} \mu_{jg}}{(\omega_{ig} - \omega)(\omega_{jg} - 2\omega)} + \text{similar terms} \qquad (4)$$

μ_{xy} is a transition dipole between states x and y. $\chi^{(2)}$, and SHG as a consequence, increases dramatically when the incoming excitation has a frequency approaching the energy of an electronic transition. This effect can be seen in equation 4 since the denominator will approach zero under such conditions. A similar result occurs when 2ω approaches a transition in the material being irradiate.

At an electrified interface, such as an electrode surface, another source of SHG is possible, the third order hyperpolarizability, equation 5.[17-19]

$$P^{3}(2\omega) = \gamma \vec{E}_{dc} (\vec{E}(\omega)\vec{E}(\omega)) + \gamma \vec{E}(\omega) (\vec{E}_{dc} \cdot \vec{E}(\omega)) \qquad (5)$$

E_{dc} is the static electric field at the surface, and γ is a term similar to $\chi^{(2)}$ in frequency dependence. Variation in SHG intensity with respect to electrode potential will be quadratic in nature with linear changes in E_{dc} unless resonance or structural effects dominate. If changes in SHG intensity are thought to be solely due to a change in E_{dc}, then identical experiments using different excitation frequencies may be performed to check any possible resonance contributions.

III. Experimental. The experimental apparatus required for generating and detecting SSHG at an interface is relatively simple. Figure 1 displays the arrangement used in studying the electrochemistry of a polycrystalline electrode.[20] The incoming laser beam radiation at frequency ω is first passed through an ω pass filter, to eliminate any harmonics due to the laser itself or any steering mirrors, and focused on to the electrode surface. The coherent 2ω signal generated closely follows the reflected incident light, allowing for easy set-up; initial detector alignment can be done using the reflected fundamental beam. The SHG signal is collimated and then focused through a 2ω pass filter, to eliminate the fundamental, and into a simple monochromator for detection. The strengths in SHG detection despite its low intensity are twofold: its coherence, we know where it is and are able to collect a large percentage of it, and its separation in frequency from the fundamental, we can eliminate virtually any signal background/noise due to scattering of the incident laser light through simple filtering methods. Most experiments using SHG as a surface probe have a similar arrangement. However, some experiments have been done in transmission.[96]

The major attraction of the SHG technique lies in its simplicity and its *in situ* capabilities. The experimental layout shown in figure 1 is easily adapted to study structure and/or kinetics. The structure can be the structure of molecules adsorbed on a liquid or solid surface, the bulk structure of solids, or the surface structure of liquids or solids at a gas/liquid, liquid/liquid, gas/solid, liquid/solid or solid/solid interface. Kinetic applications can range from the adsorption/desorption of molecules from a surface in ultra-high vacuum (UHV) studies or electrochemical studies to other reactions on surfaces, including actual reconstruction of the surface itself.

Various experimental schemes have been employed to enhance the SHG signal when dealing with polycrystalline or amorphous materials. One of the more popular methods aside from simple reflection is to employ attenuated total reflection either with single[18,21] or multiple reflections.[22]

The laser polarization and angle of incidence are important parameters even when dealing with polycrystalline or amorphous materials.[23] S-polarized radiation, $\vec{E}$ parallel to the sample surface, induces a dipole with inversion symmetry and will therefore, not generate appreciable radiation at a frequency of 2ω. P-polarized radiation, on the other hand, has $\vec{E}$ perpendicular to the surface with a non-symmetric induced dipole at the interface and will generate the largest signal possible. For the angle of incidence, the optimum SHG signal is obtained at an angle of incidence near 70° from the surface normal as predicted by theory[15,23,24] and demonstrated experimentally for both metallic[24] and non-metallic surfaces.[22]

To obtain an appreciable second harmonic signal, it is necessary to use the highest possible incoming laser intensity as possible since the SSHG signal is the result of a non-linear second order effect. Except for a few select materials with a large effective $\chi^{(2)}$ or a high resistance to thermal damage, CW and pulsed nanosecond lasers are unsuitable for routine SHG excitation due to thermal damage. Peak intensities on the order of 10^6 W/cm^2 are required for an adequate signal-to-noise ratio. Tighter focusing of these lasers to boost signal intensity on samples with a small value of $\chi^{(2)}$ concentrates too much energy for too long a time period for the material to dissipate the heat effectively. The recent introduction of commercial picosecond lasers with the requisite peak power and reasonable repetition rates has helped to circumvent this problem. The sample material being irradiated can tolerate more easily shorter pulses of the same intensity at the surface. In order to obtain the same intensity with a picosecond vs a nanosecond laser(~50 μj/90 ps pulse vs. ~1-10 mj/10 ns pulse), a smaller sampling area, an advantage if working with small samples, is necessary which decreases the SHG signal level. However, the repetition rate for the picosecond laser can be as high as ~2000 Hz vs. ~10 Hz for the nanosecond lasers, and, more importantly, higher peak intensities are possible with the picosecond laser. The irradiated sample can dissipate the heat deposited by a shorter pulse with higher intensity. As a result, a substantial gain in the second harmonic signal is achieved since it is a quadratic function of the laser intensity.

A significant advantage of using picosecond lasers in SHG work is their application to kinetic studies involving events occurring on faster time scales. The shorter the pulse, the shorter a slice in real time one is able to "freeze" and study when investigating a particular reaction. A femtosecond laser has already been used to follow the melting process of a Si single crystal when irradiated with intense light.[25]

The merit of current nanosecond lasers is their ability to deliver more power to the sample per pulse. Even though the usable peak intensity is less, the area sampled is much larger than that possible for shorter pulse lengths. Depending on the experimental requirements and equipment at hand, either laser type may be sufficient.

Further developments in laser design may greatly enhance the utility of both SHG and SFG. Pulsed tunable lasers in the visible range will be able to really exploit the resonance characteristics of $\chi^{(2)}$. By tuning the excitation frequency through the suspected transition energies for a given material,[26] true fingerprinting of compounds may be possible where more established methods have failed. SFG using one visible laser and a tunable IR laser could be used to map the vibrational structure at an interface,[27] exploiting the advantage of detection efficiency in the visible range and submonolayer detection. It might also be useful in electrochemical studies since aqueous media absorbs a negligible amount in the visible, i.e., the weak detected signal, despite strong absorption at the IR frequency where more incident power could be applied. Another wrinkle is the use of the difference in two tunable visible lasers to obtain a vibrational spectrum as demonstrated.[13]

IV. Nickel Passivation in Acid Chloride. *In-situ* characterization of the solid/liquid interface is an important challenge for the surface science community. The inherent difficulty of this measurement and the various shortcomings of presently available analysis techniques requires that relevant problems be addressed by more than one method. SSHG has demonstrated submonolayer sensitivity for many electrode processes including ionic absorption,[19,51-58] molecular adsorption,[5,11,57,59-62,65,67] underpotential deposition,[19,68,69] and for alkali metal overlayers.[70,71] Unfortunately the relationship between the observed SSHG signal intensity and the chemical identity and concentration of species at the electrode surface is a complicated one. This complexity arises from the response of SSHG signal to interfacial charge as has been described in the theory section, to electronic resonances[48,67,72-75] both in the growing film and in the substrate, and to surface morphology.[76] An additional complication is the wide, substrate dependent variation in SSHG response. The SSHG signal from an Fe surface for instance is nearly 3 orders of magnitude smaller than a Ag surface and fully 4 orders of magnitude smaller than a Ga surface.[77,78] SSHG signal from the substrate can also interfere with signal from thin films[79,80] leading to extremely complicated behaviour.

Several successful strategies have been employed to allow interpretation of the SSHG signal in terms of surface composition. Almost all electrode studies utilize information gained from cyclic voltammogram (CV) studies for clues in the interpretation of SSHG data.[1,2,20,53,54,77] Measuring the time dependence of the SSHG signal following a potential jump can provide valuable clues to the various contributions to the SSHG signal[50,61,68,81,83] The wavelength dependence of the SSHG signal has also been found to be instructive.[20,48,67,72-75]

In harsh environments Ni often forms a passive film which protects the metal from extensive corrosion. Studies of the passivation phenomena have concentrated on electrochemically-induced film formation in basic solutions[20,34-37], since such electrolytes are used in the nickel battery industry. Recently, we studied film formation[4] in chloride-containing acidic medium using *in-situ* SSHG. Although films still form on

nickel in such environments, they are not as protective against pitting-corrosion. It is well-known that chloride and other halide ions hinder passivation.[38-40] This study was useful since previous studies[33, 41-46] left unanswered many questions regarding the nature of the passivating film on nickel in acidic media. Controversy arises, in part, because of the *ex-situ* nature of surface analytical techniques and the influence of surface roughening on ellipsometric data[47].

Optical SSHG originating from the interface of a highly polished nickel electrode in acidified chloride (0.1 M NaCl, 0.01 M HCl) solution is shown in figure 4. Striking changes are observed in the SSHG signal at the onset of passive film formation for 532 nm incident light (heavy curve), while change in the SSHG signal for 1.06 μ light is delayed (light solid curve). Consider the 532 nm SSHG experiment. The peak second harmonic intensity is much less for 532 nm incident light than with 1.06 μ light, even when one takes into consideration the difference in incident laser power. In addition, the overall dependence on potential is quite different: second harmonic intensity slowly increases as the potential increases, then drops with the onset of nickel dissolution (-0.01V_{SCE}) for 532 nm light. There is a small increase in intensity shortly thereafter (at the pitting-corrosion potential) and again in the cathodic half of the cycle, which appears to occur simultaneously with the single current peak (-0.04V_{SCE}). The intensity never returns to its initial value at the beginning of the scan, although the anodic switching potential was maintained low enough to avoid serious degradation of surface quality.

With 1.06μ incident light a dramatic increase in SSHG intensity coincides with the second anodic peak in the cyclic voltammogram (CV) (+0.05V_{SCE}), and the subsequent drop on the cathodic swing occurs with the -0.04V_{SCE} peak in the CV. The sharp rise in SSHG intensity concurrent with the *second* peak in the anodic half of the cycle appears to support a dissolution-precipitation-type mechanism: presumably dissolution of the nickel (the first peak in the CV) would not change the electrical properties of the metal (although it would obviously cause some roughening of the surface) Precipitation (the second peak in the CV), on the other hand, could yield a surface film with an electronic structure very different from that of the substrate, and the dramatic change in intensity at this wavelength is suggestive of this. The fact that the SHG does not change until the *second* peak in the CV indicates that resonance enhancement does not occur until then. The sharp increase in SHG concurrent with film formation suggests that there is an electronic transition in the passive film resonant with either the incident or second harmonic light.[26,48]

These findings are consistent with the dissolution-precipitation mechanism of Reddy, Rao and Bockris.[33] and appear to indicate the presence of two distinct changes in the electronic structure of the Ni surface during anodic cycling of the Ni electrode. Detailed discussion of these results may be found elsewhere.[4]

V. Angularly Resolved Second Harmonic Generation of Fe [110] The tensorial nature of the second order nonlinear susceptibility which governs SSHG can be used to obtain structural information about an interface. The symmetry of a single crystal surface can be observed by monitoring the SHG intensity as the crystal surface is rotated about its normal. The use of various input angles and polarizations in many cases allows a fairly complete description of the symmetry of an interface. The symmetry of metal and semiconductor surfaces has been observed in UHV environments, with and without

adsorbates.[5-7,10,74,84-93,95] Also, the symmetry of a silver electrode[11,12,55,83] and a Cu electrode[94] in an electrochemical cell has been monitored as surface processes occur. These studies have demonstrated the capability of SSHG experiments to uncover the symmetry of an interface.

The structure of the oxide layers which form on iron exposed to oxygen has been explored in many UHV studies.[28-32] Several low energy electron diffraction (LEED) studies[28-32] indicate that upon submonolayer oxidation a c(2x2) overlayer is observed that transforms at elevated temperatures to a hexagonal structure. The proposed[28] surface structure for this phase is shown in figure 3. Fundamentally, the structure depicted is the [111] face of FeO single crystal. This face grows because it is in the best registry with the underlying Fe[110] substrate.

Angularly resolved SSHG studies of the air oxidized Fe[110] surface is shown in figure 4 and have been presented in detail elsewhere[3]. Because of the tensor nature of the SSHG signal the signal changes dramatically depending on the polarization of the incident 1.06 μ laser. For s- polarized near normally incident light (solid curve) a three fold symmetric pattern of the iron oxide layer is revealed. This pattern shows a slight assymettry which is more clearly evident as the incident angle is increased to 45° and 65° (not shown). The asymmetry of the three-fold pattern indicates a systematic misfit, or reconstruction of the Fe/FeO interface, to produce an apparent tilt of the three-fold axis relative to the surface normal. From a least squares fit to a model, the average tilt was found to be about 5° from the surface normal.[3]

VI. Acknowledgment This work was supported by the U.S. Department of Energy,BES-Materials Sciences under
Contract W-31-109-ENG-38.

VII. References

1. B.M. Biwer, M.J. Pellin, M.W. Schauer and D.M. Gruen, *Surf. Sci.* **176**, 377 (1986).
2. B.M. Biwer, M.J. Pellin, M.W. Schauer and D.M. Gruen, *Langmuir* **4**, 121 (1988).
3. M.W. Schauer, M.J. Pellin and D.M. Gruen, *Materials* **1**, 101 (1989).
4. J.M. Frye, M.W. Schauer, M.J. Pellin and D.M. Gruen, to be published in *Chemistry of Materials*, May/June (1990).
5. S.G. Grubb, A. M. DeSantolo, R.B. Hall *J. Phys. Chem.* **92**, 1419(1988).
6. H.W. Tom, G. D. Aumiller *Phys. Rev* **B33** 8818(1986).
7. J.A. Litwin, J.E Sipe, H.M. Van Driel *Phys Rev* **B31** 5543(1985).
8. T.F. Heinz, M.M. Loy, W. A. Thompson *Phys. Rev. Lett.* **54** 63(1985).
9. H.W. Tom, C. M. Mate, X.D. Xu, J.E. Crowell, T.F. Hienz, G.A. Samorjai, Y.R. Shen *Phys. Rev. Lett.* **52** 348(1984).
10. D. Heskett, K.J. Song, A. Burns, E.W. Plummer, H.L. Dai J.Chem. Phys. 85 7490 (1984).
11. V.L. Shannon, D.A. Koos, G.L. Richmond, *Appl. Opt.* **26** 3579(1987); *J. Phys. Chem.* **91** 5548 (1987); *J. Phys. Chem.* **87** 1440(1987); *Appl. Opt.* **26** 3579 (1987).
12. J. Miragliotta, T.E. Furtak *Phys Rev.* **B37** 1028 (1988).
13. Y.R. Shen The Principles of Nonlinear Optics, Wiley, New York 1984.
14. J.A. Armstrong, N. Bloembergen, J. Ducuing, P.S. Pershan, *Phys. Rev.* **127** 1918 (1962).

15. N. Bloembergen, P.S. Pershan, *Phys. Rev.* **128** 606(1962).
16. V. Mizrahi, J.E. Sipe *J Opt. Soc. Am.* **B5** 660 (1988).
17. C.H. Lee, R.K. Chang, N. Bloembergen, *Phys. Rev. Lett.* **18** 167 (1967).
18. C.C. Wang, *Phys. Rev.* **178** 1457(1969).
19. R.M. Corn, M. Romagnoli, M.D. Levenson, M.R. Philpott, *Chem. Phys. Lett.* **106** 30 (1984).
20. B.M. Biwer, M.J. Pellin, M.W. Schauer, D.M. Gruen *Surf. Interface Anal.* **14** 635 (1989).
21. J.C. Quail, H.J. Simon *Phys Rev* **B31** 4900 (1985).
22. G.A. Reider, A.J. Schmidt, G. Marowsky *Optics Comm.* **47** 223 (1983).
23. N. Bloembergen, R.K. Chang, S.S. Jha, C.H. Lee *Phys. Rev.* **174** 813 (1968).
24. H. Sonnenberg, H.Heffner J. Opt. Soc. Am. 58 209 (1968) and references therein.
25. C.V. Shank, R. Yen, C. Hirlimann *Phys. Rev. Lett.* **51** 900 (1983).
26. T.F. Heinz, C.K. Chen, D. Ricard, Y.R. Shen *Phys. Rev. Lett.* **48** 478 (1982).
27. X.D. Xhu, H. Suhr, Y.R. Shen *Phys. Rev.* **B35** 3047 (1987).
28. M. Langell, G.A. Samorjai, *J. Vac. Sci. Tech.*, **21** 858(1982).
29. C.R. Brundle, *Surf. Sci.* **66** 581 (1977).
30. P.B.Sewell, L.D. Stockbridge, J.M. Cohen *J.Electrochem. Soc.* **108** 933(1961).
31. H. D. Shih, F. Jona, D.W. Jepsen, P.M. Marcus *Surf.Sci* **104** 39 (1981).
32. K.O. Legg, F. Jona, D.W. Jepsen, P.M. Marcus *Phys Rev* **B16** 5271 (1977).
33. A.K.N. Reddy, M.G.B. Rao, J.O.M. Bockris *J. Chem. Phys.* **42** 2246 (1965).
34. S.U. Falk and A.J. Salkind, Alkaline Storage Batteries, Wiley, N.Y. (1969).
35. G.W.D. Briggs, Chem. Soc. Spec. Period. Rep., *Electrochemistry* **4**, 33 (1979).
36. P. Oliva, J. Leonardi, J.F. Laurent, C. Delmas, J.J. Braconnier, M. Figlarz, F. Fievet and A. deGuibert, *J. Power Sources* **8**, 229 (1982).
37. B. Beden and A. Bewick, *Electrochim Acta* **33**, 1695 (1988).
38. G.T. Burstein and G.A. Wright, *Electrochim Acta* **20,** 95 (1975).
39. B. MacDougall, *J. Electrochem. Soc.* **126,** 919 (1970).
40. Y.S. Hsu and J.K. Wu, *J. Mater. Sci. Lett.* **6**, 1246 (1987).
41. J. O'M. Bockris, A.K.N. Reddy and B. Rao, *J. Electrochem. Soc.* **113**, 1133 (1966).
42. A.K.N. Reddy and B. Rao, *Canadian J. Chem.* **47**, 2687 (1969).
43. C.Y. Chao, Z. Szklarsha-Smialowska and D.D. MacDonald, *J. Electroanal. Chem.* **131,** 289 (1982).
44. R.J. Smith, Ph.D. Thesis, University of Florida, 1984.
45. R.E. Hummel, R.J. Smith and E.D. Verink, Jr., *Corr. Sci.* **27,** 803 (1987).
46 L. Bosio, R. Cortes, P. Delichere, M. Froment and S. Joiret, *Surface and Interface Analysis* **12,** 380 (1988).
47. T. Smith, P. Smith and F. Mansfield, *J. Electrochem. Soc.* **126,** 799 (1979).
48. W. Heuer, L. Schröter and H. Zacharias, *Chem. Phys. Lett.* **135,** 299 (1987).
49. Y.R. Shen *Ann. Rev. Phys. Chem.* **40** 327 (1989).
50. G.L. Richmond, J.M. Robinson, V.L. Shannon *Progress in Surf. Sci.* **28** 1 (1988).
51. R.M. Corn, M. Romagnoli, M.D. Levenson, M.R. Philpott, *Chem. Phys. Lett.* **106** 30 (1984).
52. G.L. Richmond *Chem. Phys. Lett.* **110** 571 (1984).
53. G.L. Richmond *Langmuir.* **2** 132 (1986).
54. G.L. Richmond *Chem. Phys. Lett.* **106** 26 (1984).
55. J.M. Robinson, H.M. Rojhantalab, V.L. Shannon, G.L. Richmond *Pure and Appl. Chem.* **59** 1263 (1987).
56. X.D. Xiao, V. Vogel, Y.R. Shen *Chem. Phys. Lett.* **163** 555 (1989).
57. H.M. Rojhantalab, G.L. Richmond *J. Phys. Chem.* **93** 3269 (1989).

58. K. Bhattacharyya, A. Castro, E.V. Sitzmann, K.B. Eisenthal *J. Phys. Chem.* **89** 3376 (1988).
59. D.J. Campbell, R.M. Corn *J. Phys. Chem.* **91** 5668 (1987).
60. D.J. Campbell, D.A. Higgins, R.M. Corn *J. Phys. Chem.* **94** 3681 (1990).
61. J.M. Robinson, G.L. Richmond *Electrochim. Acta* **34** 1639 (1989).
62. R. Steinhoff, L.F. Chi, G. Marowsky, D. Moebius, *J. Opt. Soc. Amer.* **B6** 843 (1989).
63. Y. R. Shen *Nature* **337** 519 (1989).
64. V.L. Shannon, J.M. Robinson, G.L. Richmond *Spectroscopy* **3** 44 (1988).
65. D.J. Campbell, R.M. Corn *J. Phys. Chem.* **92** 5796 (1988).
66. D. Heskett, L.E. Urbach, K.J.. Song, E.W. Plummer, H.,L. Dai *Surf. Sci* **197** 225 (1988).
67. G.L. Richmond, H.M. Rojhantalab, J.M. Robinson, V.L. Shannon, *J. Opt. Soc. amer.*. **B4** 228 (1987).
68. J.M. Robinson, G.L. Richmond *Chem. Phys.* **141** 175 (1990).
69. R.M. Corn, M. Romagnoli, M.D. Levenson, M.R. Philpott, *J. Chem. Phys.* **81** 4127 (1984).
70. A. Liebsch, *Phys. Rev.* **B40** 3421 (1989).
71. K.J. Song, D. Heskett, L.E. Urbach, H.L. Dai, E.W. Plummer *Mater. Res. Soc. Symp. Proc.* **83** 259 (1987).
72. R. Georgiadis, G.A. Neff, G.L. Richmond, *J. Chem. Phys.* **92** 4623 (1990).
73. J.C. Hamilton, R.J. Anderson *J. Vac. Sci. Technol.* **7** 100 (1989).
74. J.C. Hamilton, R.J. Anderson *Thin Solid Films* **166** 345 (1988).
75. W. Heuer, L. Schröter and H. Zacharias, *Springer Ser. Opt. Sci.* **55**, 262 (1987).
76. G.L. Richmond *Chem. Phys. Lett.* **113** 359 (1985).
77. C.K. Chen,T.F. Heinz, D. Ricard, Y.R. Shen *Phys. Rev.* **B27** 1965 (1983).
78. G.T. Boyd, Th. Rasing, J.R.R.Leite, Y.R. Shen *Phys. Rev.* **B30** 519 (1984).
79. G. Berkovic, Y.R. Shen, G. Marowsky, R. Steinhoff *J. Opt. Soc. Amer.*. **B6** 205 (1989).
80. K.J. Song, D. Heskett, L.E. Urbach, H.L. Dai, A. Liebsch, E.W. Plummer *Phys. Rev. Lett.* **61** 1380 (1988).
81. L.E. Urbach, D. Heskett, J.M. Hicks, K.J.. Song, E.W. Plummer, H.,L. Dai *Proc. SPIE* **1056** 86 (1989).
82. H.W.K. Tom, *Springer Ser. Opt. Sci.* **8**, 54 (1987).
83. V.L. Shannon, D.A. Koos, J.M. Robinson, G.L. Richmond *Chem. Phys. Lett.* **142** 323 (1987).
84. D. Heskett, K. J. Song, A. Burns, E. W. Plummer, and H. L. Dai, *J. Chem. Phys.* **85**, 7490 (1986).
85. X. O. Zhu and Y. R. Shen, *Surf. Sci.* **163**, 114 (1985).
86. T. F. Heinz, M. M. T. Loy, and W. A. Thompson, *Phys. Rev. Lett.* **54**, 63 (1985).
87. H. W. K. Tom, C. M. Mate, X. D. Zhu, J. E. Crowell, T. F. Heinz, G. A. Somorjai, and Y. R. Shen, *Phys. Rev. Lett.* **52**, 348 (1984).
88. H. W. K. Tom, T. F. Heinz, and Y. R. Shen, *Phys. Rev. Lett.* **51**, 1983 (1983).
89. J.C. Hamilton, L.R. Williams, R.J. Anderson *Chem. Phys. Lett.* **167** 507 (1990).
90. M.L. Lynch, R.M. Corn *J. Chem. Phys.* **94** 4382 (1990).
91. G. Luepke, G. Marowsky, R. Steinhoff, *Phys. Rev. B.* **41** 6913 (1990).
92. Z. Rosenzwieg, M. Asscher *Surf. Sci.* **225** 249 (1990).
93. A. Friedrich, B. Pettinger, D.M. Kolb,G. Luepke, R. Steinhoff, G. Marowsky, *Chem. Phys. Lett* **163** 123 (1989).
94. V.L. Shannon, D.A. Koos, S.A. Kellar, P. Huifang, G.L. Richmond J *Phys. Chem.* **93** 6434 (1989).

95. J.C. Hamilton, R.J. Anderson *Chem. Phys. Lett* **151** 455 (1988); *Phys Rev. B* **38**.8451 (1988).
96. N. Bloembergen, H.J. Simon, C.H. Lee *Phys. Rev.* **181** 1261 (1969).

Figure 1. Top view of an experimental apparatus for SSHG detection in reflection from a polycrystalline electrode surface.

Figure 2. Cyclic voltammogram (CV; light broken line) and second harmonic intensity of a polycrystalline Ni surface. The heavy line is for an incident wavelength of 1.06 μm. The three dot dash heavy line is for an incident wavelength of 532 nm and is 1/10 the intensity of the second SSHG curve.

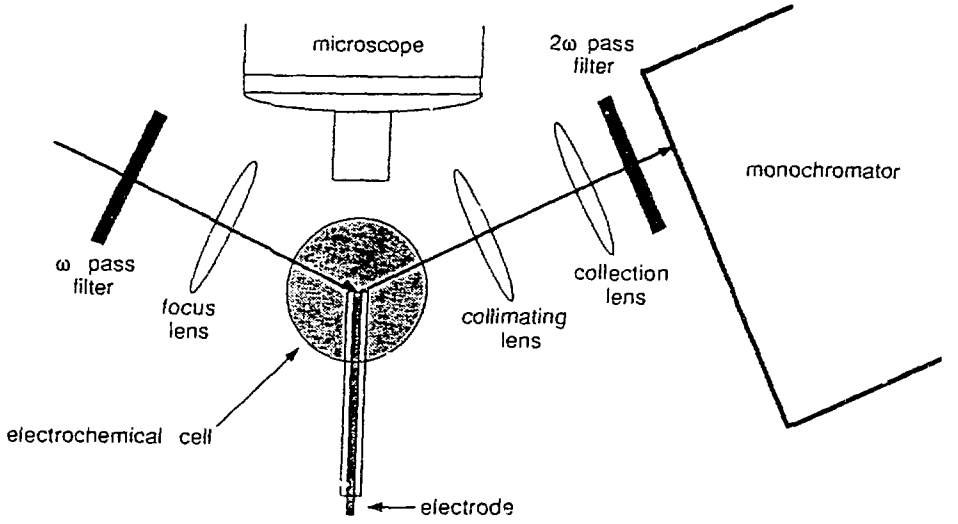

Figure 1. Top view of an experimental apparatus for SSHG detection in reflection from a polycrystalline electrode surface.

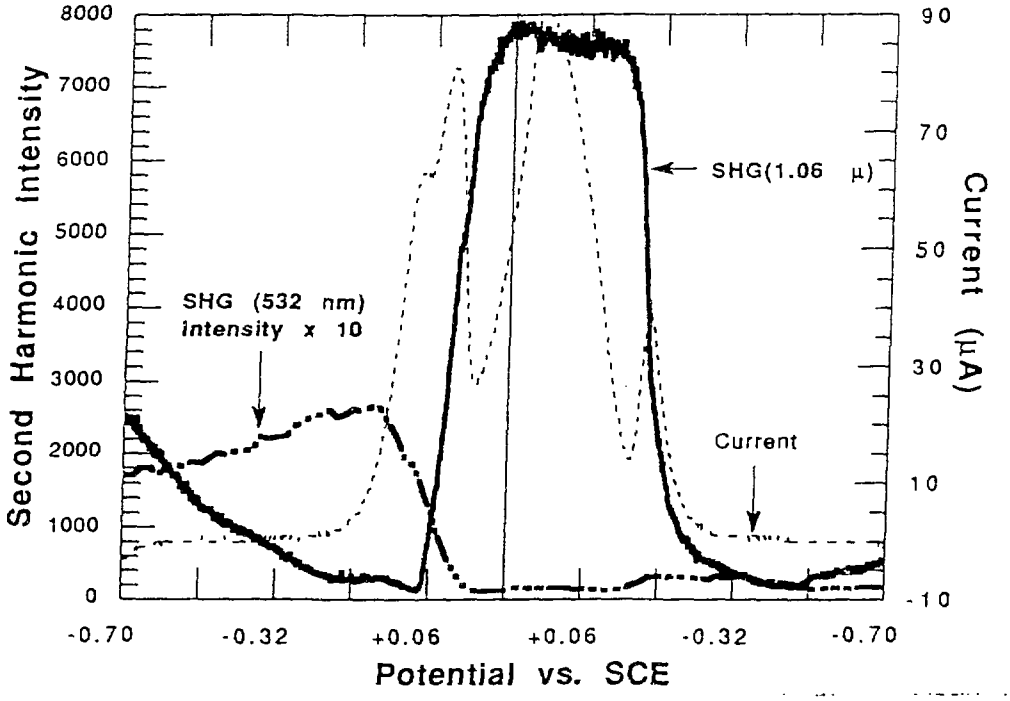

Figure 2. Cyclic voltammogram (CV; light broken line) and second harmonic intensity of a polycrystalline Ni surface. The heavy line is for an incident wavelength of 1.06 μm. The three dot dash heavy line is for an incident wavelength of 532 nm and is 1/10 the intensity of the second SSHG curve.

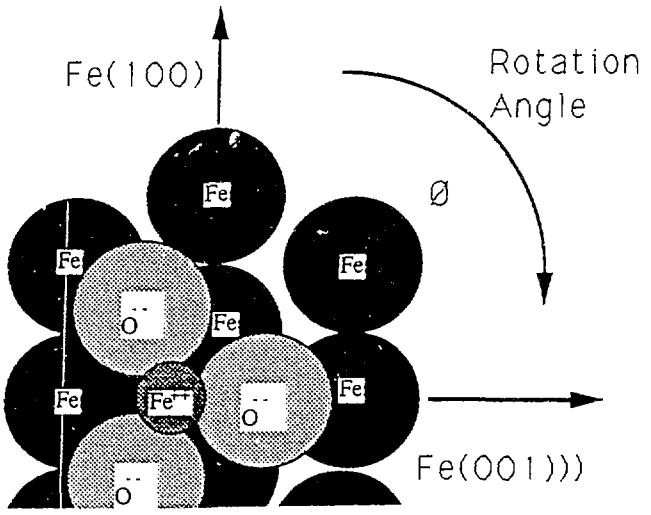

Figure 3. Structural diagram of the Fe/FeO surface. The dark circles represent Fe^{0}; the light grey circles O^{-}; and the dark grey(smallest) circles represent Fe^{++}. The FeO phase shown is the [111] face.

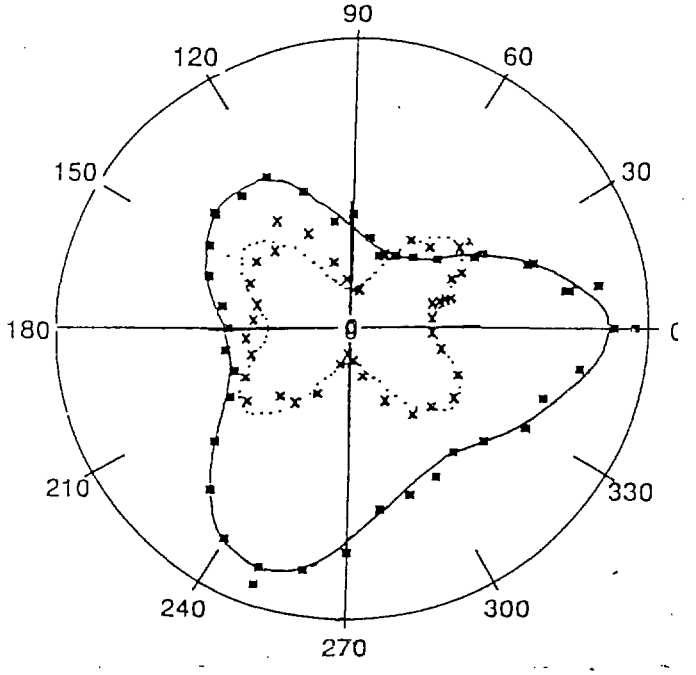

Figure 4. SSHG intensity plotted as a function of rotation of the Fe [110] surface about its normal. The Fe [001] direction is taken as 0°. The dotted curve and the "x" data points is for p polarized incident light and p polarized second harmonic light. This spectra shows the bulk bilateral symmetry of the Fe [110] substrate. The solid curve is for an s polarized incident beam and a p polarized second harmonic signal. Here the three fold symmetry of the FeO [111] surface can be found.